IOP Conf. Series: Materials Science and Engineering **123** (2016) 012030 doi:10.1088/1757-899X/123/1/012030

Effect of temperature and concentration of precursors on morphology and photocatalytic activity of zinc oxide thin films prepared by hydrothermal route

S Heinonen[1], J-P Nikkanen[1], H Hakola[2], E Huttunen-Saarivirta[3], M Kannisto[2], L Hyvärinen[1], M Järveläinen[1], E Levänen[1]

[1]Department of Materials Science, Tampere University of Technology Tampere, Finland
[2]Department of Chemistry and Bioengineering, Tampere University of Technology Tampere, Finland
[3]VTT Technical Research Centre of Finland, Materials Performance, Tampere, Finland

E-mail: saara.heinonen@tut.fi

Abstract Zinc oxide (ZnO) is an important semiconductive material due to its potential applications, such as conductive gas sensors, transparent conductive electrodes, solar cells, and photocatalysts. Photocatalytic activity can be exploited in the decomposition of hazardous pollutants from environment. In this study, we produced zinc oxide thin films on stainless steel plates by hydrothermal method varying the precursor concentration (from 0.029 M to 0.16 M) and the synthesis temperature (from 70˚C to 90 ˚C). Morphology of the synthesized films was examined using field-emission scanning electron microscopy (FESEM) and photocatalytic activity of the films was characterized using methylene blue decomposition tests. It was found that the morphology of the nanostructures was strongly affected by the precursor concentration and the temperature of the synthesis. At lower concentrations zinc oxide grew as thin needlelike nanorods of uniform length and shape and aligned perpendicular to the stainless steel substrate surface. At higher concentrations the shape of the rods transformed towards hexagon shaped units and further on towards flaky platelets. Temperature changes caused variations in the coating thickness and the orientation of the crystal units. It was also observed, that the photocatalytic activity of the prepared films was clearly dependent on the morphology of the surfaces.

1. Introduction

The state of environment is one of the most important issues faced by modern society. Sufficiency and availability of energy and water as well as environmental pollution are today's main concerns. Industrial growth caused by increased consumption has resulted in severe environmental problems due to the release of harmful and toxic substances into water and air. This has led to development of cheap and effective technologies to remove and destroy the toxins and pollutants. [1–5]

Since 1972 when Fujishima and Fonda [6] discovered that titanium dioxide can split water into hydrogen and oxygen under ultraviolet illumination, TiO2 photocatalysis has been widely studied and its efficiency in mineralization of severe organic pollutants as well as bacteria and other organic contamination has been recognized. [7–14] Another wide band gap (3.37 eV) semiconductor material

that has recently attained focus due to its photocatalytic ability is zinc oxide. In addition to photocatalytic properties, nanostructured ZnO has optical and electrical properties which make it suitable for several potential applications, e.g., solar cells, gas sensors, piezoelectric materials and ceramic devices. ZnO nanostructures, such as nanotubes, nanosheets, nanowires, mesoporous films, nanorods and nanoparticles have been synthetized using different methods and results have been widely reported. [1, 15–23] It has also been shown that structure directing agents, such as ethanol and urea, can be used to control the formation of ZnO structures. [23–24] Photocatalytic performance depends on the crystal structure and the composition of the material. Since photocatalysis is a surface controlled mechanism, increase in the surface area emphasizes the photoactivity of the material. [25–26]

In this study, we have used hydrothermal method to produce nine different ZnO coatings each with unique nanostructure by varying synthesis temperature and precursor concentration. The aim of the study was to investigate the effect of surface morphology on photocatalytic performance of the ZnO coatings.

2. Experimental

2.1. Preparation and characterization of zinc oxide films

Zinc oxide films were prepared by a two-step hydrothermal method. At first, a seed layer was formed on an AISI 304 stainless steel (SS) substrate (75mm x 25 mm) followed by the growth of ZnO nanorods. Before the process, substrates were cleaned by wiping with 2-propanol (C3H7OH, 99.5 %, VWR) and then rinsed with ethanol (C2H5OH, 99.5 %, Altia Oyj). A solution for the seed layer was prepared mixing 2-methoxyethanol (CH3OCH2CH2OH, ≥99,5%, Sigma-Aldrich) and ethanolamine (NH2CH2CH2OH, ≥ 99.0 %, Sigma-Aldrich) (96:4) and dissolving 0.23 M zinc acetate ($C_4H_6O_4Zn \cdot 2H_2O$, ≥ 98%, Sigma-Aldrich) into the mixture. Solution was then stirred at 60ºC for 2 h. After cooling down, the solution was spin coated (1500 rpm, 20 s) on the substrates and then the samples were heat treated at 350 ºC for 20 min. The solution for growth of ZnO layer with nanotopography was prepared mixing hexamethylenetetramine (C6H12N, 99%, Sigma-Aldrich) and zinc nitrate (Zn(NO3)2, 98%, Sigma-Aldrich) volume ratio being 1:1. The concentrations were 0.029 M, 0.058 M and 0.16 M. Coatings were fabricated at three temperatures: 70ºC, 80ºC and 90ºC. The plates were placed in the solution the seed layer side upside down and the growth was carried out for 2 hours. After removing the samples from the solution they were rinsed with de-ionized water and dried in air. The samples were finally heat-treated at 300ºC for 30 min.

The prepared zinc oxide films were characterized using field emission scanning electron microscopy (FESEM, Zeiss ULTRAplus) for surface morphology studies, energy-dispersive X-ray spectroscopy (EDS, INCA Energy 350) for elemental analysis and X-Ray diffraction (XRD, Panalytical Empyrean Multipurpose Diffractometer) to define the crystal structure of the samples.

2.2. Photocatalytic measurements

Photocatalytic measurements were performed in an aqueous solution of methylene blue (MB). The sample plates were placed in a decanter glass with 30 ml of 0.0085 mM MB solution. In order to reach adsorption equilibrium, the test solution was first kept in the dark for 60 min after which the ultra violet (UV)-lamp was turned on. Illumination was done from above with a 100 W/m2 power using Ledia NIS330U-M UV-Gun (peak maximum at 365 ± 5 nm). The concentration of MB in the solution was followed by UV-VIS spectroscopy (Shimadzu UV-2501PC Spectrophotometer). At one hour intervals a 3 ml MB solution was taken for absorbance measurement. The absorbance was measured at the wavelength of 665 nm. A dark experiment without any irradiation but under otherwise identical without sample plates was also tested to confirm that irradiation does not compose MB intrinsically.

Photocatalytic activity of the coatings was also tested by irradiating the samples with UV-light of 50W/m^2 power with the same equipment described above. Coatings were irradiated for 30 min and the water contact angle (WCA) was measured after 10, 20 and 30 min of irradiation.

3. Results and discussion

3.1. Morphology and crystal structure of ZnO films grown in different precursor concentration solutions and temperatures

Nine types of ZnO coatings were prepared varying synthesis temperature and precursor concentration. Samples prepared at precursor concentration of 0.029 M at 70ºC, 80ºC and 90ºC are denoted as $C_1$70, $C_1$80 and $C_1$90, respectively. Samples prepared at precursor concentration of 0.058 M at 70ºC, 80ºC and 90ºC are denoted as $C_2$70, $C_2$80 and $C_2$90, respectively, and samples prepared at precursor concentration of 0.16 M at 70ºC, 80ºC and 90ºC are denoted as $C_3$70, $C_3$80 and $C_3$90, respectively. Both synthesis temperature and precursor concentration impacted significantly the final nanotopography of the surfaces (Fig. 1–3). Sample $C_1$70 was only partly covered by small nano-sized nubs which were mostly concentrated on the grain boundaries of the stainless steel. This may be explained by the fact that the grain boundaries are often thermodynamically favourable nucleation sites [27] and the low temperature and precursor concentration were not sufficient for nucleation at more energetically demanding surface nucleation sites. The same effect could be seen with samples $C_1$80 and $C_1$90: the coating was thickest and the structure most uniform at the grain boundaries whereas some small uncoated areas were observed in the middle of the grains.

Sample $C_2$70 had flat hexagonal crystals whereas samples $C_2$80 and $C_2$90 consisted of hexagonally shaped rods. The structure of $C_2$80 was dense and the rods grew perpendicularly to the substrate contrary to the rods of $C_2$90 that had approximately the same rod diameter but the rods were pointing irregularly to different directions (Fig. 2c). This phenomenon was also distinguished with the sample $C_1$90. On samples $C_3$70, $C_3$80 and $C_3$90, ZnO formed a flaky structure flake size being highest at $C_3$90. The flaky morphology is probably due to the high precursor concentration which led to fast nucleation at several different sites resulting in less organized structure as compared to $C_2$80 and $C_2$90. Nucleation also occurred to a great extent in the solution which could be observed during the synthesis as ZnO powder precipitated on the bottom of the synthesis container.

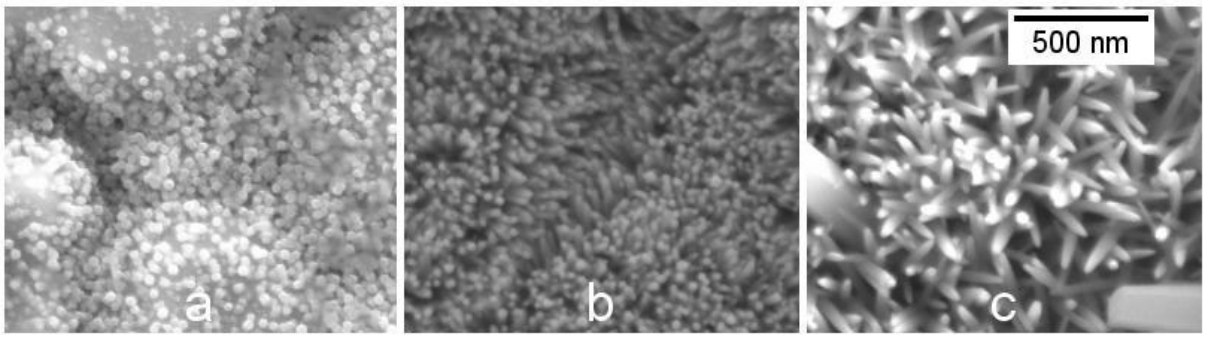

Figure 1 a–c. FESEM images of ZnO coatings grown at a) 70°C, b) 80°C and c) 90°C precursor concentration being 0.029 M (C1).

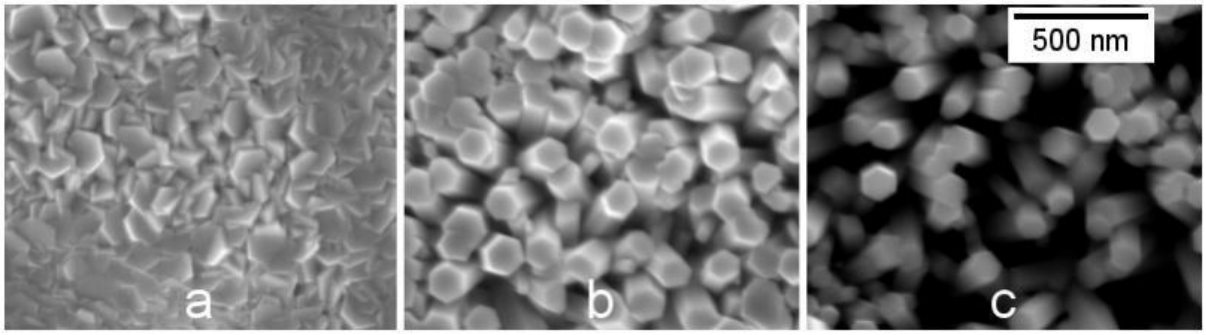

Figure 2 a–c. FESEM images of ZnO coatings grown at a) 70°C, b) 80°C and c) 90°C precursor concentration being 0.058 M (C2).

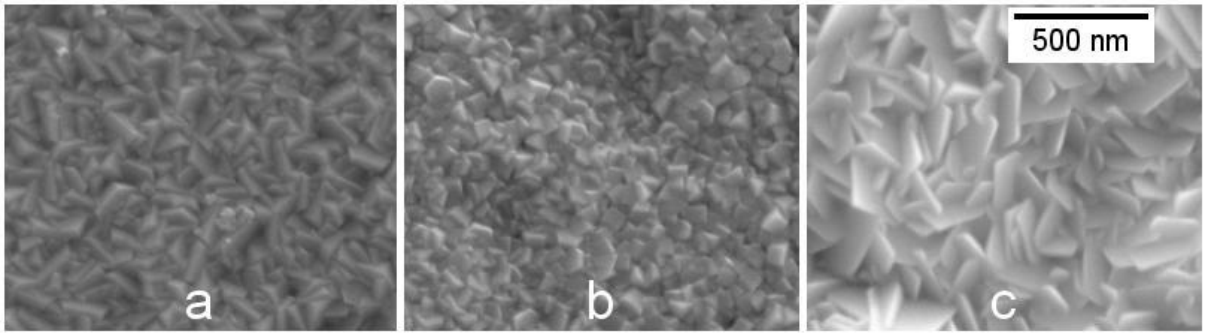

Figure 3 a–c. FESEM images of ZnO coatings grown at a) 70°C, b) 80°C and c) 90°C precursor concentration being 0.16 M (C3)

The thicknesses of the coatings were investigated by imaging the cross-sections of the coated plates (Table 1). The thicknesses were of the same magnitude (1.1–1.6 μm) for $C_1$80, $C_1$90, $C_2$80 and $C_2$90. Instead, for $C_1$70, $C_2$70, $C_3$70 and $C_3$80, the coating thicknesses were in the range of 180–300 nm, i.e., much smaller than in the other cases. For $C_3$90, the coating thickness was 630 nm. The lower thicknesses of $C_3$70, $C_3$80 and $C_3$90 can be explained with the nucleation occurring in the solution leading to less molecules precipitating on the surface and forming the coating. With $C_1$70, $C_2$70 and $C_3$70, the low thickness is probably due to the low temperature, which decelerates or hinders the reaction.

Table 1. Coating thicknesses of the prepared samples

c (mol/l)	70°C	80°C	90°C
0.29 M	180 nm	1380 nm	1100 nm
0.58 M	230 nm	1100 nm	1600 nm
0.16 M	300 nm	210 nm	630 nm

XRD analyses were conducted for all nine coatings and all of them showed clear peaks of hexagonal wurtzite structure. Apart from peaks of wurtzite and stainless steel substrate, no other peaks were found. EDS analyses were in of line with the received XRD patterns showing peaks of Zn, O and peaks resulting from the stainless steel substrate.

3.2. MB degradation results

The dark tests performed before the actual measurements showed that the concentration of the solution did not change during one hour in dark and thus the samples did not adsorb methylene blue. It is also notable that the irradiation of MB without the samples did not influence the concentration of MB, which means that irradiation did not intrinsically decompose MB. Based on MB degradation test results, the sample $C_2$90 had the highest photocatalytic activity although all the prepared coatings showed relatively good photocatalytic performance (Fig. 4). The difference between samples $C_2$80 and $C_2$90 could be due to the more randomly oriented structure of $C_2$90 leading $C_2$90 to have larger surface area being in contact with the MB-solution. The nanorods of the sample $C_2$80 seem to have fused together particularly near the substrate but also partly all the way along the rods. The same explanation could be applied to the difference in the photocatalytic activity between the coatings $C_1$80 and $C_1$90.

The results obtained from the WCA measurements of the irradiated coatings (Table 2) were consistent with the MB degradation results. Reference stainless steel substrate did not show any change in water contact angle during the irradiation test. In contrast, complete wetting of the surface was obtained after 30 min of irradiation with UV-light with samples $C_1$90, $C_2$90 and $C_3$80 which can be attributed to high photocatalytic activity of the films. Some questions still remain, since the sample $C_3$80 was clearly less efficient at MB degradation test (76 % of the MB degraded after 7 h of

irradiation) compared to C290 (91 % of the MB degraded after 7 h of irradiation) but it showed omplete wetting of the surface after 30 min of irradiation along with $C_1$90 and $C_2$90. In our future studies, it is essential to explain these observations.

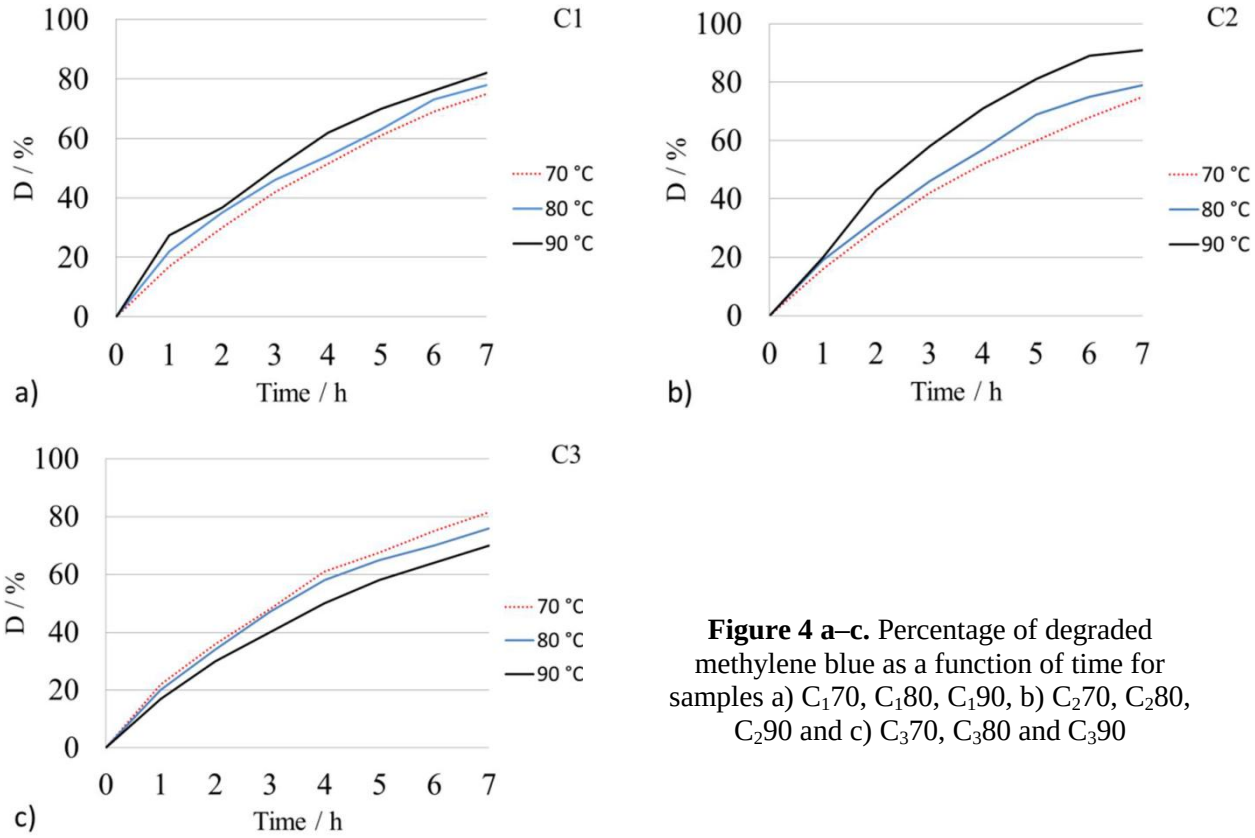

Figure 4 a–c. Percentage of degraded methylene blue as a function of time for samples a) $C_1$70, $C_1$80, $C_1$90, b) $C_2$70, $C_2$80, $C_2$90 and c) $C_3$70, $C_3$80 and $C_3$90

Table 2. Water contact angles of stainless steel and the ZnO coatings after 0, 10, 20 and 30 min irradiation with UV-light

Sample	0 min (°)	10 min (°)	20 min (°)	30 min (°)
$C_1$70	40	26	16	6
$C_1$80	20	4	10	7
$C_1$90	78	9	0	0
$C_2$70	83	32	25	22
$C_2$80	81	28	22	10
$C_2$90	61	12	0	0
$C_3$70	35	11	8	7
$C_3$80	71	15	12	0
$C_3$90	76	60	39	21
SS	77	78	70	78

The results presented in this paper could be concluded as follows: 1) both concentration of the precursor solution and synthesis temperature have a notable impact on the surface morphology and coating thickness. At lower concentrations the structure of the surface is needle-like and it changes towards hexagonal shaped units as the concentration increases. Finally, when the concentration is further increased, the surface changes from hexagonal units to flaky structure due to the rapid nucleation in the solution. 2) Although all the tested coatings showed relatively good photocatalytic

performance, the activity is clearly related to nanostructure of the coatings. Indeed, the high photocatalytic activity of the two most active coatings can be explained by fragment position of ZnO nanorods which obviously enhances the surface area of the coatings. In addition to the impact of surface area, the polarity difference in different crystal orientations of the nano-sized crystals could also affect the photocatalytic performance due to different adsorption properties of different plains. This will be investigated more in forthcoming studies.

References

[1] Khan R, Hassan M S, Cho H-S, Polyakov A Y, Khil M-S and Lee I-H 2014 *Mater. Lett.* **133** 224
[2] Gürlük S 2009 *Ecol Econ* **68** 2327
[3] Loganathan N, Shahbaz M and Taha R 2014 *Renew. Sust. Energ. Rev.* **38** 1083
[4] Barakat M A 2011 *Arabian Journal of Chemistry* **4** 361
[5] Aarthi T and Madras G 2008 *Catal. Commun.* **9** 630
[6] Fujishima A and Honda K 1972 *Nature* **238** 37
[7] Wang Y, Zhu S, Chen X, Tan Y, Jiang Y, Peng Z and Wang H 2014 *Appl. Surf. Sci.* **307** 263
[8] Yu T, Tan X, Zhao L, Yin Y, Chen P and Wei J 2010 *Chem. Eng. J* **157** 86
[9] Yang J, Bai H, Tan X and Lian J 2006 *Appl. Surf. Sci*. **253** 1988
[10] Nikkanen J-P, Huttunen-Saarivirta E, Zhang X, Heinonen S, Kanerva T, Levänen E and Mäntylä T 2014 *Ceram. Int.* **40** 4429
[11] Goswami D Y, Trivedi D and Block S S 1997 *J. Solar. Energy Eng.* **119** 92
[12] Jacoby W A, Maness P, Wolfrum E J, Blake D M, Fennell J A 1998 *Environ. Sci. Technol.* **32** 2650
[13] Vohra A, Goswami D Y, Deshpande D A and Block S S 2006 *Appl. Catal. B-Environ.* **65** 57
[14] L Zhong, F Haghighat and C-S Lee 2013 *Build. Environ.* **62** 155
[15] Saarenpää H, Niemi T, Tukiainen A, Lemmetyinen H and Tkachenko N 2010 *Sol. Energ. Mat. Sol. C* **94** 1379
[16] Saarenpää H, Sariola-Leikas E, Pyymäki Perros A, Kontio J M, Efimov A, Hayashi H, Lipsanen H, Imahori H, Lemmetyinen H and Tkachenko N V 2012 *J. Phys. Chem. C* **116** 2336
[17] Polsongkram D, Chamninok P, Pukird S, Chow L, Lupan O, Chai G, Khallaf H, Park S and Schulte A 2008 *Physica B* **403** 3713
[18] Eswar K A, Rouhi J, Husairi F S, Dalvand R, Alrokayan S A H, Khan H A, Rusop Mahmood M and Abdullah S 2014 *J. Mol. Struct.* **1074** 140
[19] Zhou Y, Liu C, Zhong X, Wu H, Li M and Wang L *Ceram. Int.* **40** 10415
[20] Chen X, Zhai Y, Li J, Fang X, Fang F, Chu X, Wei Z and Wang X 2014 *Appl. Surf. Sci.* **319** 216
[21] Koao L F, Dejene F B and Swart H C 2014 *Mat. Sci. Semicon. Proc.* **27** 33
[22] J Gupta, Bhargava P and Bahadur D 2014 *Physica B* **448** 16
[23] Zhu Y F, Fan D H, Dong Y W and Zhou G H 2014 *Superlattice Microst.* **74** 261
[24] Foe K, Namkoong G, Abdel-Fattah T M, Baumgart H, Jeong M S and Lee D S 2013 *Thin solid films* **534** 76
[25] Nikkanen J-P, Heinonen S, Huttunen-Saarivirta E, Honkanen M and Levänen E 2013 *IOP Conf. Ser.: Mater. Sci. Eng.* **47** 012066
[26] Maury-Ramirez A, Nikkanen J-P, Honkanen M, Demeestere K, Levänen E and De Belie N 2014 *Mater. Charact.* **87** 74
[27] Ng H T, Li J, Smith M K, Nguyen P, Cassell A, Han J and Meyyappan M 2003 *Science* **300** 1249